Energy materials

CrossMark

Prussian blue analogues-derived bimetallic phosphide hollow nanocubes grown on Ni foam as water splitting electrocatalyst

Gang Yan[1],* iD, Xiaotong Zhang[1], and Liguang Xiao[1],*

[1] *College of Material Science and Engineering, Jilin Jianzhu University, Changchun 130118, People's Republic of China*

ABSTRACT

The development of highly active and stable electrocatalysts for the water splitting using the earth-abundant transition metal as precursor is important for the renewable energy application. Prussian blue analogues (PBAs) are regarded as an ideal precursor for the preparation of electrocatalysts because of its abundant metal elements and various derived porous nanostructures. In this work, the $(NiCo)_2P$ hollow nanocubes, which are firmly grown on Ni foam, are prepared by PBAs and used as an water splitting electrocatalyst with high activity and stability in 1 M KOH solution. Benefiting from the synergistic effect of nickel and cobalt, hollow structure and high double-layer capacitance, the as-synthesized $(NiCo)_2P$/NF catalyst shows an excellent electrocatalytic performance for the water splitting. To achieve current density of 10 mA cm^{-2}, for HER and OER, this material requires overpotentials of 162 mV and 220 mV, respectively. As an integrated electrocatalyst for water splitting, the $(NiCo)_2P$/ NF needs a cell voltage of 1.62 V to achieve current density of 10 mA cm^{-2}. Furthermore, this material has long-term electrocatalytic stability (over 30 h). The high catalytic activity of this material is attributed to the synergistic effect of component and the hollow structure of catalyst. This facile and novel method of preparing bimetallic phosphide electrocatalysts with hollow structure provides a broadened space for the design and synthesis of non-noble metal catalysts in the future.

Introduction

Electrocatalytic water splitting to produce H_2 and O_2, as one of the promising methods to resolve the energy consumption, has attracted increasing attention [1, 2]. The water splitting is composed of two half-reactions of hydrogen evolution reaction (HER) and oxygen evolution reaction (OER). These reactions should be driven by effective catalysts with high activity, long-term stability and low cost [3]. The noble metal catalyst such as Pt is the most effective

Address correspondence to E-mail: yang431@nenu.edu.cn; xlg627@163.com

🍂 Springer

HER catalyst, and Ir/Ru is the state-of-the-art OER catalyst. However, the scarcity and high cost of noble metal catalysts restrict their widespread application. Various types of transition metal catalysts have been developed as a substitute for the noble metal [4–8]. The unique electrocatalytic properties of transition metal phosphide have attracted wide attention in the past few years. Among them, bimetallic phosphide, such as Ni–Co–P, has been explored as promising electrocatalyst in the water splitting [9, 10]. Compared with monometallic catalysts, the mixed metal catalysts exhibit enhanced activities due to the increased number of active sites and the synergistic effects of components [11, 12]. However, the limited active area of electrodes and the number of exposed active sites of most reported bimetallic phosphides result in poor catalytic activity. It remains a great challenge to design and synthesize catalysts with high active area.

Metal–cyanide compound, i.e., Prussian blue analogues (PBAs) with abundant element composition (Ni, Co, Fe, Cu, Mn et al.), and various derivative structures (microboxes, hollow cage or frame and core–shell structure) have been widely studied in the field of electrocatalysis and energy conversion/storage [13–20]. The abundant metal composition of PBAs makes them an excellent precursor for the design and synthesis of bimetallic/polymetallic catalysts. Furthermore, the controllable pyrolysis of PBAs at high temperature results in various porous nanostructures with high surface area. Therefore, the PBAs should be an ideal precursor to prepare hollow bimetallic phosphides catalysts with high active area and active sites. However, the poor electrical conductivity of metallic phosphides and the weakness of traditional powder materials, such as cumbersome and time-consuming electrode preparation process, extra added polymeric binders, easy peeling of coated materials, limit them for large-scale practical applications [21]. Recently, catalysts directly grown on self-supporting electrodes have attracted widespread attention. Compared with traditional powder materials, self-supporting electrode materials have many advantages, such as enhanced electron conductivity, larger electrode area and high mechanical stability. Many studies have shown that the PBAs nanoparticle catalysts grown in situ on self-supporting electrodes have enhanced catalytic activity and stability [22–24]. Hence, by fine-tuning the metal species and phosphating conditions, hollow bimetallic phosphide electrocatalysts grown on self-supporting electrodes in situ can be obtained and show promising applications in the field of electrocatalysis.

Herein, a nickel–cobalt phosphide bimetallic hollow catalyst in situ grown on a Ni foam (abbr. $(NiCo)_2P/NF$) is fabricated by means of phosphating method using PBAs $Ni_3[Co(CN)_6]_2$ as precursors. The as-synthesized $(NiCo)_2P/NF$ catalyst shows an excellent electrocatalytic performance for the water splitting under alkaline conditions. To achieve current density of 10 mA cm^{-2}, for HER and OER, this material requires overpotentials of 162 mV and 220 mV, respectively. As an integrated electrocatalyst for water splitting, the $(NiCo)_2P/NF$ needs a cell voltage of 1.62 V to achieve current density of 10 mA cm^{-2}. Furthermore, this material has long-term electrocatalytic stability (over 30 h). The high catalytic activity and stability of this material are contributed to the synergistic effect of component and the hollow structure of catalyst and the strong adhesion between catalysts and Ni foam. This facile and novel method of preparing bimetallic phosphide electrocatalysts with hollow structure provides a broaden space for the design and synthesis of non-noble metal catalysts in the future.

Results and discussion

The preparation of $(NiCo)_2P/NF$ contains two steps and is shown in Fig. 1 and supporting information. First, the $Ni_3[Co(CN)_6]_2$ nanocubes on the surface of the Ni foam are prepared by a facile coprecipitation method using Ni foam immersed in the mixed solution of Ni^{2+} and $[Co(CN)_6]^{3-}$. The second step is using NaH_2PO_2 as phosphorus source to calcinate the $Ni_3[Co(CN)_6]_2/NF$ precursor at low temperature. The hollow bimetallic phosphide $(NiCo)_2P/NF$ is obtained after calcination at 350 °C in N_2 atmosphere. Thermogravimetric (TG) test of $Ni_3[Co(CN)_6]_2$ is conducted to understand the formation mechanism of the hollow bimetallic phosphide. The TG curve of $Ni_3[Co(CN)_6]_2$ is shown in Fig S1; $Ni_3[Co(CN)_6]_2$ suffers clear weight loss below 300 °C, which should be attributed to the removal of crystallized water and coordinating water in $Ni_3[Co(CN)_6]_2$. The second weight loss in the range of 300–500 °C, which is ascribed to the decomposition of cyanogens ligands (CN). The CN group decomposed and further

Figure 1 A schematic diagram of preparation of hollow $(NiCo)_2P/NF$ nanocubes grown on Ni foam.
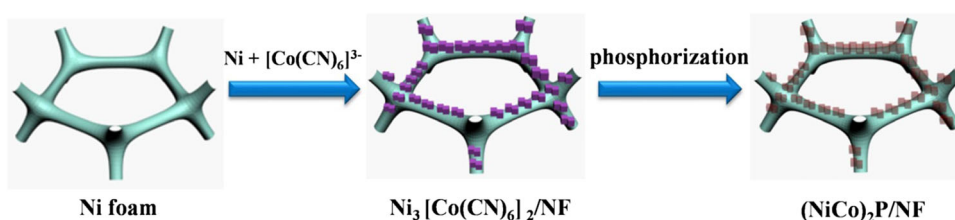
released carbon/nitrogen oxide, which leads to the final hollow nanostructure of bimetallic phosphide. The XRD patterns of $Ni_3[Co(CN)_6]_2/NF$ and $(NiCo)_2P/NF$ are shown in Fig. 2. The diffraction peaks at 44.9°, 52.2° and 76.6° are indexed to the substrate of Ni foam. The diffraction peaks of $Ni_3[Co(CN)_6]_2/NF$ are in good agreement with the standard diffraction patterns of $Ni_3[Co(CN)_6]_2$ (JCPDS No. 89-3738), which indicates that the PBAs nanocrystals have been successfully prepared. The main diffraction peaks of $(NiCo)_2P/NF$ can be matched with Ni_2P (JCPDS No. 65-9706). Because the partial substitution of Ni ions by Co ions does not affect the crystal structure, there are just only slight changes in the lattice parameters (Fig. 2b).

The valence states and surface compositions of $(NiCo)_2P/NF$ are investigated by X-ray photoelectron spectroscopy (XPS) analysis. The survey XPS spectrum shows the element of C, O, Ni, Co and P (Fig. 3a). The Ni $2p$ XPS spectrum is deconvoluted into six peaks, and the binding energies at 852.4 eV and 870 eV are attributed to the Ni–P species (Fig. 3b) [25]. The peaks located at binding energies of 855.9 eV and 873.8 eV with satellite peaks at 861.5 eV and 879.7 eV are assigned to the Ni–O species. The Co $2p$ XPS spectrum is deconvoluted into six peaks.

The binding energies at 778.1 eV and 793.0 eV are attributed to the Co–P species (Fig. 3c). The peaks located at binding energies of 782.0 eV and 797.2 eV with satellite peaks at 786.8 eV and 800.6 eV are assigned to the Co–O species [26]. The Ni/Co–O metal oxides are resulted from the superficial oxidation of bimetallic phosphide $(NiCo)_2P/NF$ when it is exposed in the air condition [27]. The P $2p$ XPS spectrum is shown in Fig. 3d, and the peaks with binding energies of 129.2 eV and 133.3 eV are attributed to the P–Ni/Co and P–O species, respectively [28].

The morphology and structure of the obtained materials are characterized by scanning electron microscopy (SEM) and transmission electron microscopy (TEM). The SEM images of $Ni_3[Co(CN)_6]_2/NF$ are shown in Fig. 4a, S2. It is obvious that the $Ni_3[Co(CN)_6]_2$ nanocubes on the Ni foam surface have a cubic morphology with an average size approximately 50 nm and smooth surfaces. After phosphidation at low temperature, the morphology of as-obtained $(NiCo)_2P$ bimetallic phosphide nanocubes becomes irregular and the surface becomes rough (Fig. 4b). The TEM image (Fig. 4c) clearly shows that the $(NiCo)_2P$ bimetallic phosphide has a hollow structure. The organic ligand cyanogens decompose
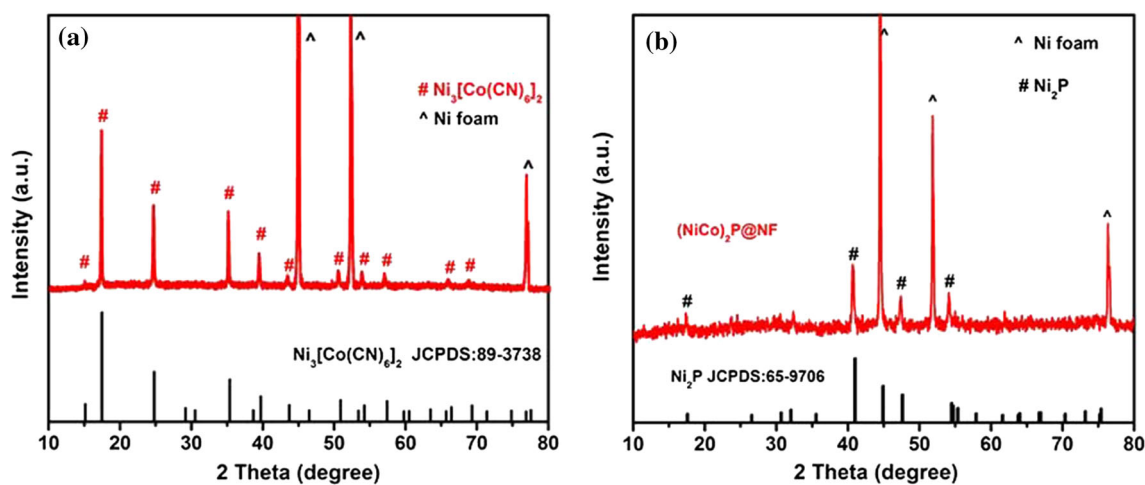

Figure 2 **a** XRD patterns of $Ni_3[Co(CN)_6]_2/NF$ and **b** $(NiCo)_2P/NF$.

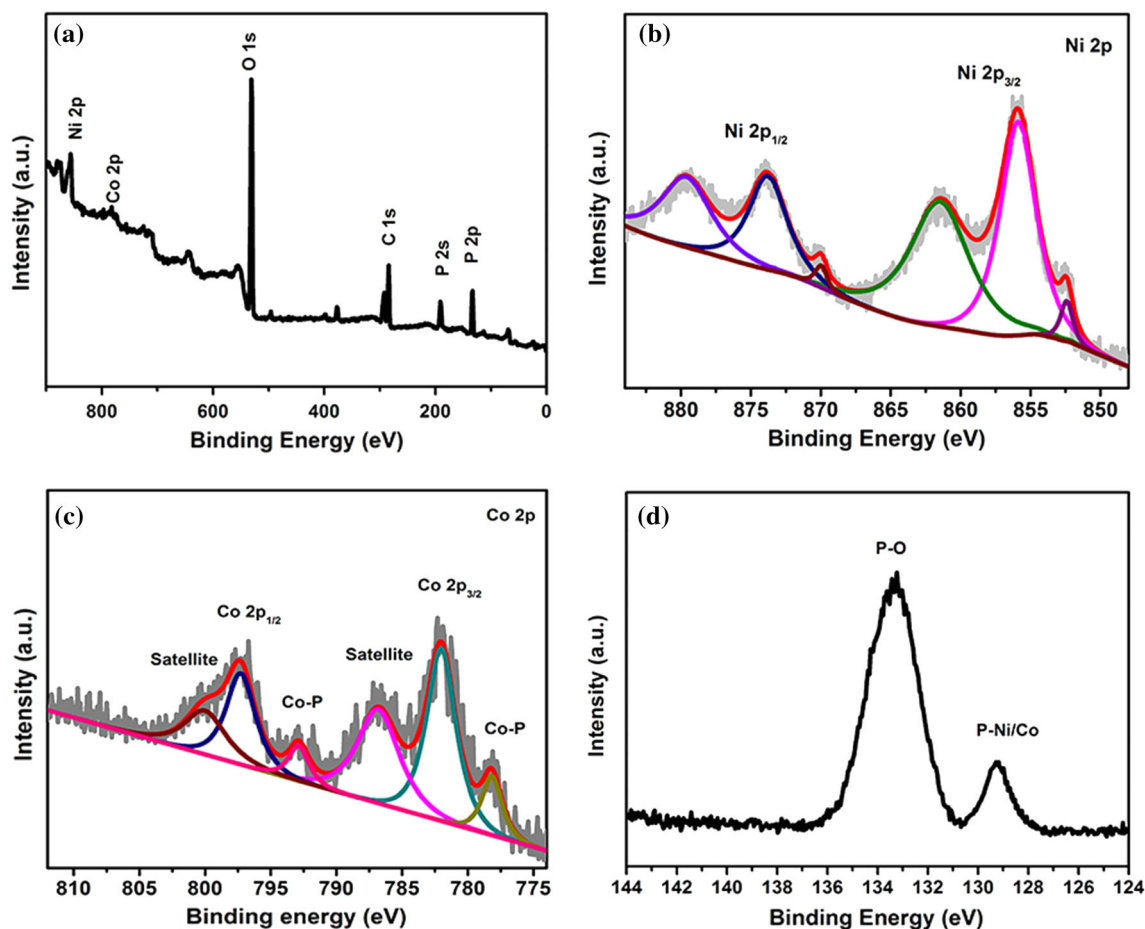**Figure 3** XPS spectrum of **a** survey spectral, **b** Ni 2*p*, **c** Co 2*p* and **d** P 2*p* of (NiCo)$_2$P/NF.

and release C and N oxide gases under heating, resulting in the hollow nanocubes structure. The hollow structural feature of (NiCo)$_2$P is beneficial to increase the active area of materials, which can expose more active sites and accelerate the mass/electron transfer. The HRTEM image is shown in Fig. 4d. The lattice fringes with interplanar distance of 0.221 nm are observed obviously, corresponding to the (111) plane of Ni$_2$P (Fig. 3e). The HRTEM result is in agreement with the XRD results. The SEM image and associated element mappings show that Ni, Co, O and P elements are distributed throughout the materials (Fig. 4e, f).

The electrocatalytic performance of the (NiCo)$_2$P/NF catalyst and the control samples for oxygen evolution reaction (OER) were evaluated in an N$_2$-saturated 1 M KOH solution. The IrO$_2$, Ni$_3$[Co(CN)$_6$]$_2$/NF and NF are also tested for comparison. The catalysts grown on Ni foam are directly used as working electrodes with a typical three-electrode electrochemical system in the CHI 760E electrochemical station. The counter electrode and the reference electrode are carbon rods and saturated calomel electrodes, respectively. The OER linear sweep voltammetry (LSV) polarization curves for these catalysts are depicted in Fig. 5a. The polarization curves show that the (NiCo)$_2$P/NF requires lower overpotential (220 mV) than IrO$_2$ (330 mV), Ni[Fe(CN)$_6$]/NF (340 mV) and NF (400 mV) to drive the current density of 10 mA cm^{-2}. The anode current density of (NiCo)$_2$P/NF increases rapidly. The (NiCo)$_2$P/NF can deliver a current density of 100 and 300 mA cm^{-2} at overpotential of 360 mV and 530 mV. Furthermore, the Tafel plots derived from OER polarization curves are used to evaluate the OER kinetics of these catalysts. As shown in Fig. 5b, the Tafel slope of the (NiCo)$_2$P/NF (69 mV dec^{-1}) is smaller than the control samples of IrO$_2$ (74 mV dev^{-1}), Ni$_3$[Co(CN)$_6$]$_2$/NF (117 mV dec^{-1}) and NF (125 mV dec^{-1}). The lower Tafel slope of the
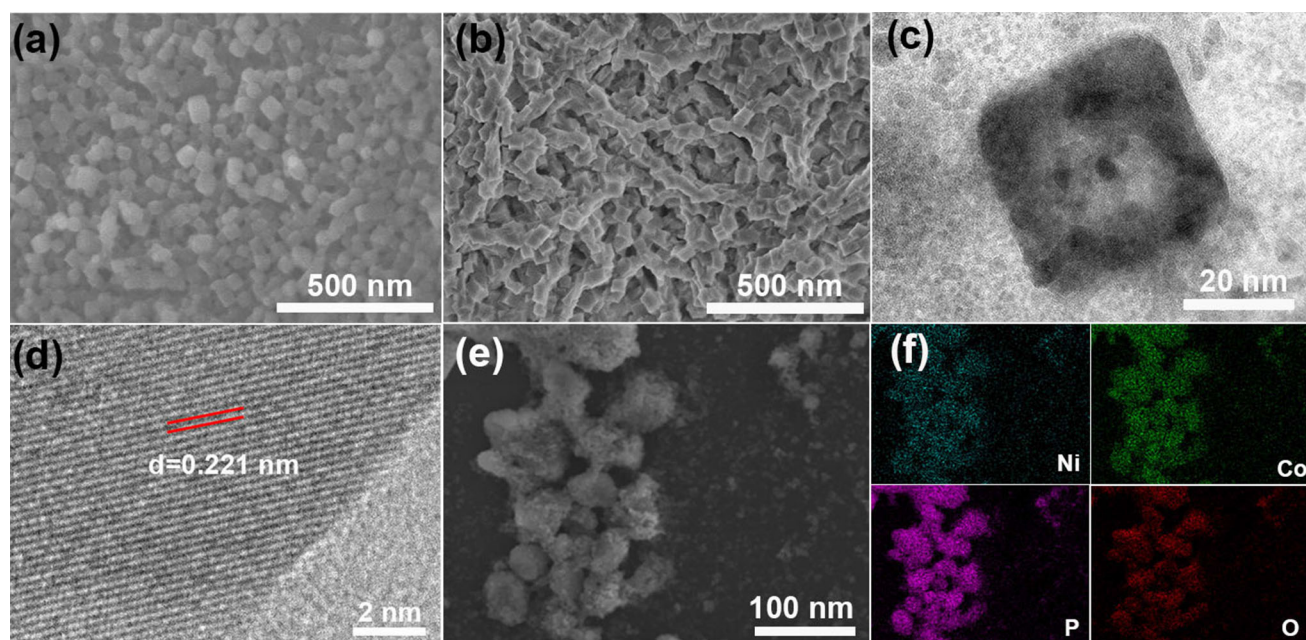
Figure 4 **a** The SEM image of Ni$_3$[Co(CN)$_6$]$_2$/NF and **b** (NiCo)$_2$P/NF, **c** TEM image of (NiCo)$_2$P/NF, **d** HRTEM image of (NiCo)$_2$P/NF, **e** and **f** the corresponding element mappings of Ni, Fe, O and P.

(NiCo)$_2$P/NF indicates the more favourable kinetics and faster electron transport for the (NiCo)$_2$P/NF than other control samples. The fast reaction kinetics of the (NiCo)$_2$P/NF should be assigned to the hollow structure of (NiCo)$_2$P with enhanced charge transfer ability. The OER performance of the (NiCo)$_2$P/NF catalyst is favourably comparable to those of other reported non-noble metal OER catalysts (Table S1). In addition, the hollow structure of (NiCo)$_2$P/NF gives the catalyst higher double-layer capacitance (16.7 mF cm^{-2}) than other control samples, such as IrO$_2$ (10 mF cm^{-2}), Ni$_3$[Co(CN)$_6$]$_2$/NF (3.2 mF cm^{-2}) and NF (1.7 mF cm^{-2}). The high double-layer capacitance of the (NiCo)$_2$P/NF helps to expose more active sites and accelerate the mass/charge transfer (Fig. 5c, d). In order to further provide an insight into the electrode reaction kinetics of the catalysts, the electrochemical impedance spectroscopy (EIS) is studied. The Nyquist plots of the catalysts are shown in Fig. 5e, and the charge transfer resistance (R_{ct}) order is: (NiCo)$_2$P/NF < Ni$_3$[Co(CN)$_6$]$_2$/NF < NF. The observed semicircles are attributed to the charge transfer resistance (R_{ct}) between the interface of electrode and electrolyte. The R_{ct} value of (NiCo)$_2$P/NF is 10.6 Ω, much smaller than that of other samples. These results indicate that the rapid charge transfer reaction kinetics occur at the (NiCo)$_2$P/NF–electrolyte interface. The low charge transfer resistance of (NiCo)$_2$P/NF is in good consistency with the Tafel slopes and LSV curve results discussed before. Such low charge transfer resistance benefits for the charge transfer and reaction kinetics. Finally, the long-term stability of (NiCo)$_2$P/NF is investigated by chronoamperometry at a certain potential. The i–t curve is shown in Fig. 5f, and the (NiCo)$_2$P/NF retains its current density of 110 mA cm^{-2} over 30 h. These results suggest that the (NiCo)$_2$P/NF is highly stable, which is important for its industrial application.

The electrocatalytic performance of the (NiCo)$_2$P/NF catalyst and the control samples for hydrogen evolution reaction (HER) is further evaluated in 1 M KOH solution. The LSV curves are shown in Fig. 6a. As expected, the Pt/C has the best HER performance with the smallest overpotential of 29 mV to reach 10 mA cm^{-2}. The (NiCo)$_2$P/NF exhibits the superior electrocatalytic activity with lower overpotential (η_{10}) of 162 mV to achieve 10 mA cm^{-2}, which is substantially lower than that of Ni$_3$[Co(CN)$_6$]$_2$/NF (226 mV) and NF (287 mV). Furthermore, the current density of (NiCo)$_2$P/NF increases rapidly with the increase in potential and exceeds that of Pt/C at high overpotential (− 310 mV). The Tafel slopes can reflect the intrinsic activities and HER mechanism of electrocatalysts under equilibrium conditions. As shown in Fig S3,
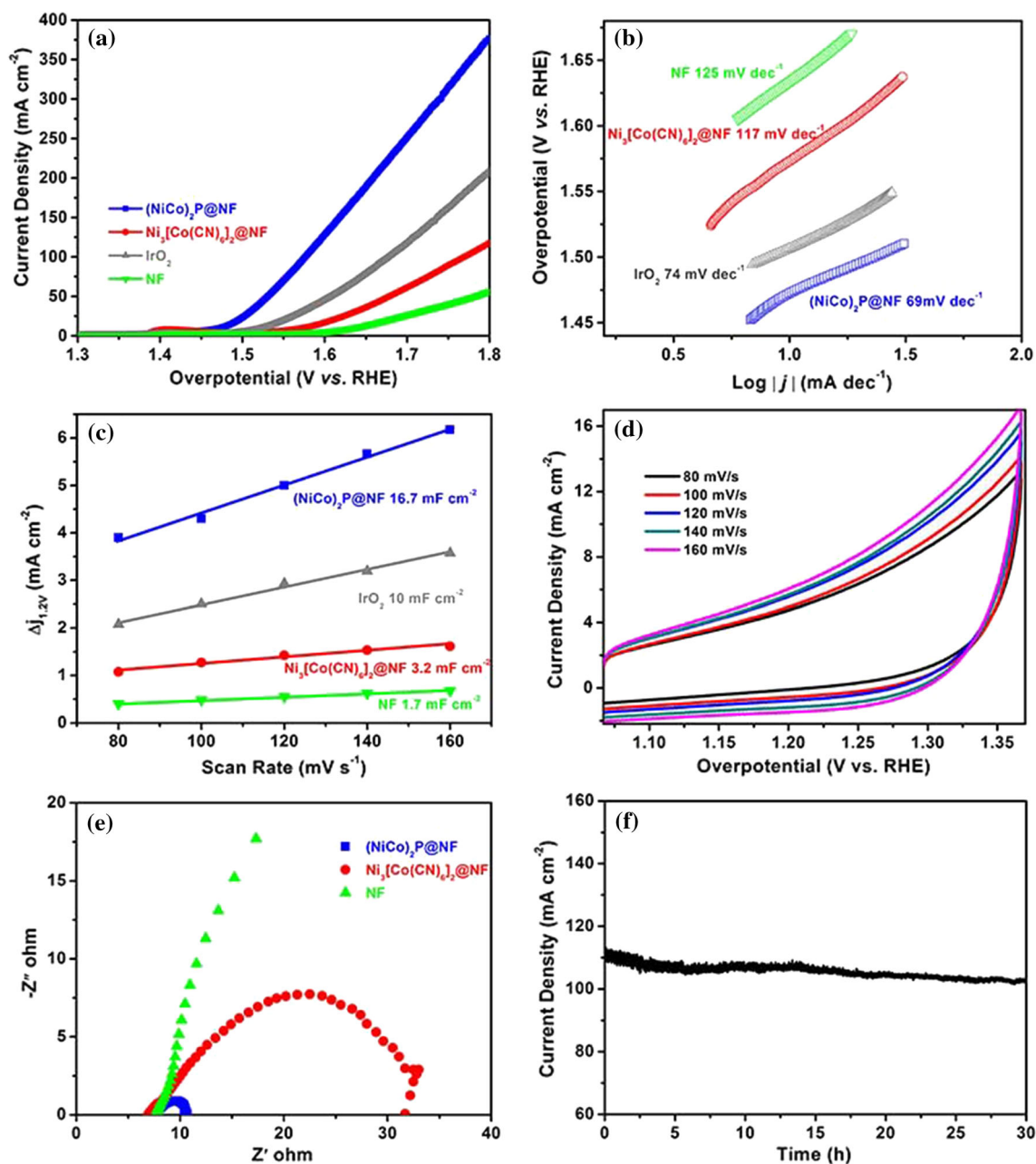
Figure 5 a The OER polarization curves of (NiCo)$_2$P/NF, Ni$_3$[Co(CN)$_6$]$_2$/NF, IrO$_2$ and NF. **b** The corresponding Tafel slope plots. **c** The current density differences Δj plotted against scan rates. **d** Cyclic voltammograms (CVs) of (NiCo)$_2$P in 1 M KOH solution. **e** Nyquist plots of samples at potential of 1.7 V (vs. RHE). **f** i–t curves of (NiCo)$_2$P/NF in 1 M KOH at overpotential of 350 mV.

the Tafel slope of the (NiCo)$_2$P/NF (135 mV dec^{-1}) is smaller than that of the control samples of Ni$_3$[Co(CN)$_6$]$_2$/NF (172 mV dec^{-1}) and NF (237 mV dec^{-1}). The lower Tafel slope of (NiCo)$_2$P/NF indicates that the HER on (NiCo)$_2$P/NF proceeds via the Volmer–Heyrovsky mechanism and the rate-limiting step is electrochemical desorption. Such

lower Tafel slope also indicates the remarkable reaction kinetics and rapid hydrogen generation for HER. The stability of electrocatalyst is an important factor to determine whether it can be used in practical applications. Therefore, the chronoamperometry test of the (NiCo)$_2$P/NF is performed at an overpotential of 320 mV. The i–t curve shows that the current

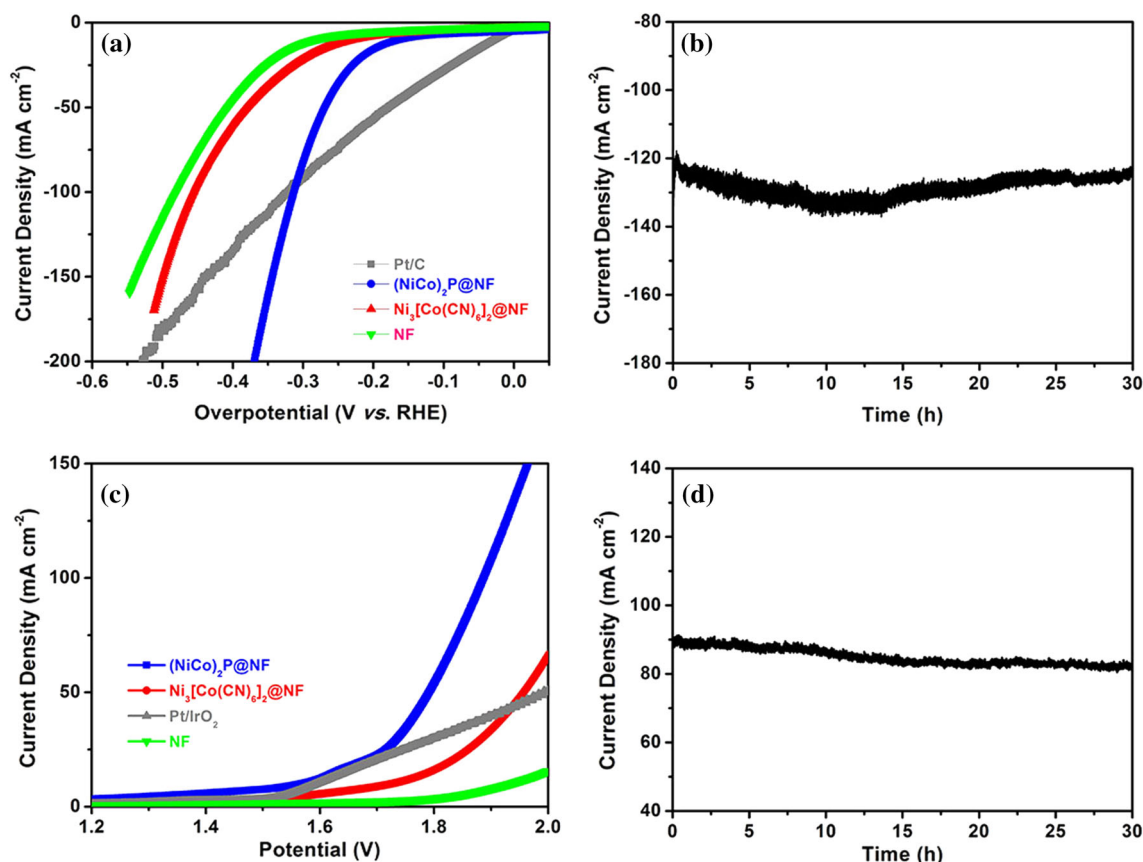**Figure 6 a** The HER polarization curves of Pt/C, $(NiCo)_2P/NF$, $Ni_3[Co(CN)_6]_2/NF$ and NF in 1 M KOH solution. **b** i–t curves of $(NiCo)_2P/NF$ for HER in 1 M KOH at overpotential 340 mV.

c The LSV curves of catalysts for water splitting in 1 M KOH. **d** i–t curve of $(NiCo)_2P/NF$ as cathode and anode at constant potential 1.82 V.

density decrease in $(NiCo)_2P/NF$ is negligible after 30-h electrocatalysis (Fig. 6b). The above-mentioned electrocatalytic results indicate that the $(NiCo)_2P/NF$ should be a highly active and stable bifunctional electrocatalyst used as both anodic and cathodic electrodes for OER and HER in water splitting. To verify this hypothesis, a two-electrode integrated electrolyser with $(NiCo)_2P/NF$ as anode and cathode is assembled in 1 M KOH solution. As shown in Fig. 6c, the $(NiCo)_2P/NF$ catalyst exhibited high activity for overall water splitting with the voltage of 1.62 V to reach 10 mA cm^{-2}, which dramatically lower than that of noble metal catalyst Pt/C–IrO$_2$ (1.6 V), $Ni_3[Co(CN)_6]_2/NF$ (1.73 V) and NF (1.93 V). The electrocatalytic performance of the $(NiCo)_2P/NF$ is comparable to that of other non-noble metal catalysts (Table S1). Furthermore, the $(NiCo)_2P/NF$ also maintained superior stability, as confirmed by the chronoamperometry curve at 90 mA cm^{-2} for 30 h (Fig. 6d). Such high efficiency and long-term stability

of electrocatalytic performance make the $(NiCo)_2P/NF$ have potential to replace the noble metals catalysts in the field of electrocatalytic overall water splitting.

The $(NiCo)_2P$ hollow nanocubes grown on Ni foam used as electrocatalyst exhibited competitive HER, OER and water splitting performance. The superior performance of $(NiCo)_2P/NF$ can be interpreted by the following items: (1) the synergistic effects of transition metals (Ni, Co) with intrinsic high catalytic activity; (2) the unique porous hollow nanostructure of metal phosphide that provided abundant accessible active sites and high surface area, which is beneficial for the adequate contact between the electrolytes and the active sites. (3) Compared with metal oxides, the metal phosphides have optimized electronic structure and enhanced conductivity, which makes them have better catalytic activity for water splitting. (4) The hollow metal phosphide nanocubes are firmly grown on the conductive

porous Ni foam substrate, which not only helps to improve the catalytic activity, but also enhances the stability of the electrode material, so that it has good prospects for large-scale application.

Conclusion

In summary, the unique bimetallic phosphide hollow nanocubes firmly grown on Ni foam $(NiCo)_2P/NF$ as bifunctional electrocatalysts for overall water splitting have been prepared by phosphorization $Ni_3[Co(CN)_6]_2/NF$. The hierarchically porous structure of the as-obtained materials can reduce charge/mass transfer resistance and promote the generated gas diffusion. Benefiting from the synergistic effect of nickel and cobalt, hollow structure and high double-layer capacitance, the as-synthesized $(NiCo)_2P/NF$ catalyst shows an excellent electrocatalytic performance for the water splitting. To achieve current density of 10 mA cm^{-2}, for HER and OER, this material requires overpotentials of 162 mV and 220 mV, respectively. As an integrated electrocatalyst for water splitting, the $(NiCo)_2P/NF$ needs a cell voltage of 1.62 V to achieve current density of 10 mA cm^{-2}. Furthermore, this material has long-term electrocatalytic stability (over 30 h). This facile and novel method of preparing bimetallic phosphide electrocatalysts with hollow structure based on the Prussian blue analogues provides a new strategy for the design and synthesis of metal catalysts for replacing precious metals in the future.

Acknowledgements

Electronic supplementary material: The online version of this article (https://doi.org/10.1007/s108 53-019-03362-6) contains supplementary material, which is available to authorized users.

References

[1] Wang H, Xu S, Tsai C, Li Y, Liu C, Zhao J, Liu Y, Yuan H, Abild-Pedersen F, Prinz FB, Nørskov JK, Cui Y (2016) Direct and continuous strain control of catalysts with tunable battery electrode materials. Science 354(6315):1031–1036

[2] Huang X, Zhao Z, Cao L, Chen Y, Zhu E, Lin Z, Li M, Yan A, Zettl A, Wang YM, Duan X, Mueller T, Huang Y (2015) High-performance transition metal-doped Pt_3Ni octahedra for oxygen reduction reaction. Science 348(6240):1230–1234

[3] Walter MG, Warren EL, McKone JR, Boettcher SW, Mi Q, Santori NS, Lewis EA (2010) Solar water splitting cells. Chem Rev 110(11):6446–6473

[4] Yu XY, Feng Y, Guan BY, Lou XWD, Paik U (2016) Carbon coated porous nickel phosphides nanoplates for highly efficient oxygen evolution reaction. Energy Environ Sci 9(4):1246–1250

[5] Zhang W, Wu YZ, Qi J, Chen MX, Cao R (2017) A thin NiFe hydroxide film formed by stepwise electrodeposition strategy with significantly improved catalytic water oxidation efficiency. Adv Energy Mater 7(9):1602547

[6] Hu F, Zhu SL, Chen SM, Li Y, Ma L, Wu TP, Zhang Y, Wang CM, Liu CC, Yang XJ, Song L, Yang XW, Xiong YJ (2017) Amorphous metallic NiFeP: a conductive bulk material achieving high activity for oxygen evolution reaction in both alkaline and acidic media. Adv Mater 29(32):1606570

[7] Xie LS, Zhang R, Cui LA, Liu DN, Hao S, Ma YJ, Du G, Asiri AM, Sun XP (2017) High-performance electrolytic oxygen evolution in neutral media catalyzed by a cobalt phosphate nanoarray. Angew Chem Int Ed 56(4):1064–1068

[8] Guo CX, Zheng Y, Ran JR, Xie FX, Jaroniec M, Qiao SZ (2017) Engineering high-energy interfacial structures for high-performance oxygen-involving electrocatalysis. Angew Chem Int Ed 56(29):8539–8543

[9] Du YM, Li ZJ, Liu YR, Yang Y, Wang L (2018) Nickel–iron phosphides nanorods derived from bimetallic-organic frameworks for hydrogen evolution reaction. Appl Surf Sci 457:1081–1086

[10] Cao LM, Hu YW, Tang SF, IIjin A, Wang JW, Zhang ZM, Lu TB (2018) Fe-CoP electrocatalyst derived from a bimetallic Prussian blue analogue for large-current-density oxygen evolution and overall water splitting. Adv Sci 5(10):1800949

[11] Zhang FS, Wang JW, Luo J, Liu RR, Zhang ZM, He CT, Lu TB (2017) Extraction of nickel from NiFe–LDH into $Ni_2P@NiFe$ hydroxide as a bifunctional electrocatalyst for efficient overall water splitting. Chem Sci 9(5):1375–1384

[12] Tan JB, Sahoo P, Wang JW, Hu YW, Zhang ZM, Lu TB (2017) Highly efficient oxygen evolution electrocatalysts prepared by using reduction-engraved ferrites on graphene oxide. Inorg Chem Front 5(2):310–318

[13] Nai JW, Lu Y, Yu L, Wang X, Lou XWD (2017) Formation of Ni–Fe mixed diselenide nanocages as a superior oxygen evolution electrocatalyst. Adv Mater 29(41):1703870

[14] Yu XY, Yu L, Wu HB, Lou XWD (2015) Formation of nickel sulfide nanoframes from metal–organic frameworks with enhanced pseudocapacitive and electrocatalytic properties. Angew Chem Int Ed 54(18):5331–5335

[15] Fang YJ, Yu XY, Lou XWD (2018) formation of hierarchical Cu-doped $CoSe_2$ microboxes via sequential ion exchange for high-performance sodium-ion batteries. Adv Mater 30(21):1706668

[16] Kang BK, Woo MH, Lee J, Song YH, Wang ZL, Guo YN, Yamauchi Y, Kim JH, Lim B, Yoon DH (2017) Mesoporous Ni–Fe oxide multi-composite hollow nanocages for efficient electrocatalytic water oxidation reactions. J Mater Chem A 5(9):4320–4324

[17] Guo YN, Tang J, Wang ZL, Kang YM, Bando Y, Yamauchi Y (2018) Elaborately assembled core-shell structured metal sulfides as a bifunctional catalyst for highly efficient electrochemical overall water splitting. Nano Energy 47:494–502

[18] Zhu XH, Liu MJ, Liu Y, Chen RW, Nie Z, Li JH, Yao SZ (2016) Carbon-coated hollow mesoporous FeP microcubes: an efficient and stable electrocatalyst for hydrogen evolution. J Mater Chem A 4(23):8974–8977

[19] Sivanantham A, Ganesan P, Estevez L, Mcgrail BP, Motkuri RK, Shanmugam S (2018) A stable graphitic, nanocarbon-encapsulated, cobalt-rich core-shell electrocatalyst as an oxygen electrode in a water electrolyzer. Adv Energy Mater 8(14):1702838

[20] Cai XJ, Gao W, Ma M, Wu MY, Zhang LL, Zheng YY, Chen HR, Shi JL (2015) A Prussian blue-based core-shell hollow-structured mesoporous nanoparticle as a smart theranostic agent with ultrahigh pH-responsive longitudinal relaxivity. Adv Mater 27(41):6382–6389

[21] Ma TY, Dai S, Qiao SZ (2016) Self-supported electrocatalysts for advanced energy conversion processes. Mater Today 19(5):265–273

[22] Indra A, Paik U, Song T (2018) Boosting electrochemical water oxidation with metal hydroxide carbonate templated Prussian blue analogues. Angew Chem Int Ed 57(5):1241–1245

[23] Guo TR, Wang T, Chen J, Zheng J, Li XG, Ostrikov K (2018) Air plasma activation of catalytic sites in a metal–cyanide framework for efficient oxygen evolution reaction. Adv Energy Mater 8(18):1800085

[24] Ge YC, Dong P, Craig SR, Ajayan PM, Ye MX, Shen JF (2018) Transforming nickel hydroxide into 3D Prussian blue analogue array to obtain Ni_2P/Fe_2P for efficient hydrogen evolution reaction. Adv Energy Mater 8(21):1800484

[25] Stern LA, Feng LG, Song F, Hu XL (2015) Ni_2P as a Janus catalyst for water splitting: the oxygen evolution activity of Ni_2P nanoparticles. Energy Environ Sci 8(8):2347–2351

[26] Liang H, Gandi AN, Anjum DH, Wang X, Schwingenschlögl HN, Alshareef U (2016) Plasma-assisted synthesis of NiCoP for efficient overall water splitting. Nano Lett 16(12):7718–7725

[27] You B, Jiang N, Sheng ML, Bhushan MW, Sun YJ (2016) Hierarchically porous urchin-like Ni_2P superstructures supported on nickel foam as efficient bifunctional electrocatalysts for overall water splitting. ACS Catal 6(2):714–721

[28] Yu XY, Feng Y, Guan BY, Lou XW, Paik U (2016) Carbon coated porous nickel phosphides nanoplates for highly efficient oxygen evolution reaction. Energy Environ Sci 9(4):1246–1250